Core–Shell Latex Particles Containing a Fluorinated Polymer in the Shell. I. Film Formation Studied by Fluorescence Nonradiative Energy Transfer

PIERRE MARION,[1] GÉRARD BEINERT,[1] DIDIER JUHUÉ,[2] JACQUES LANG[1]

[1] Institut Charles Sadron (CRM-EAHP), CNRS-ULP Strasbourg, 6, rue Boussingault, 67083 Strasbourg Cédex, France

[2] ELF-Atochem, CERDATO, LEM, 27470 Serquigny, France

Received 22 September 1996; accepted 30 November 1996

ABSTRACT: The core–shell morphology of polyacrylate latex particles containing a fluoropolymer in the shell was characterized via the fluorescent nonradiative energy transfer (NRET) technique. This technique enables one to follow the extent of mixing of fluorescently labeled latex particles during film formation. The comparison between the film formation behavior of fully labeled core–shell particles and partially labeled (no probe in the shell) core–shell particles showed evidence of the core–shell morphology of our particles. © 1997 John Wiley & Sons, Inc. J Appl Polym Sci **64:** 2409–2419, 1997

INTRODUCTION

Core–shell latex particles have many applications in the chemical, biological, and pharmaceutical industries. In the chemical industry, for instance, they are often designed to confer different properties to a final material. In the original core–shell particle, one of these properties is carried by the core and the other by the shell. This implies that the polymers forming the core and the shell are somewhat different in nature (T_g, chemical composition). Therefore, in the final material, i.e., after film formation, the polymer chains of the original particles are rarely totally mixed, but form, rather, a heterogeneous material where the two types of polymers can be distributed in various fashions. The polymer originally comprising the shell can form, e.g., a uniform matrix in which the cores stay intact and are uniformly distributed in the matrix. This happens, for instance, when the T_g of the core is higher, and the T_g of the shell, lower, than the temperature at which the film is prepared.

Another example is when the polymers forming the core and the shell phase separate totally or partially in the film. Due to differences in hydrophobicity or in surface tension, one of the polymers might preferentially migrate to the surface during film formation. The migration of one of the polymers to the surface can present a great economical advantage in surface coating if this polymer is expensive.[1] Indeed, only a small quantity of this polymer (originally in the shell for instance) will then be needed. This polymer will confer on the surface the desired property (hydrophobicity, light reflection), while the other polymer (originally in the core) will then serve, e.g., as a mechanical support for the coating. They are two main objectives to be considered in this kind of problem: (i) first to try to tailor structured particles in which one polymer is at the center of the particle and the other polymer is at the periphery and (ii) next to obtain the desired polymer, and, thus, the desired property, at the surface of the final film. The aim of the work presented here was to examine the first aspect of this problem.

The synthesis of core–shell particles is not straightforward and its success depends on many parameters, as, for instance, the method of syn-

Correspondence to: J. Lang.
Contract grant sponsor: Elf Atochem.

thesis (batch, stage polymerization, semicontinuous), the degree of incompatibility between the shell– and the core–polymer or their glass transition temperature, T_g, the relative affinity of these polymers for the water phase, the relative solubility of the monomers in water, or the relative interfacial tension between the two polymers and between each polymer and the water phase. Although rationalization of the morphology of composite particles was suggested by Sundberg and collaborators,[2,3] prediction of the morphology of core–shell particles is not easy and this is why many methods are employed to try to determine the internal structure of core–shell latex particles. Among these methods, the most often used is transmission electron microscopy (TEM), which is also one of the first methods employed for this purpose in the early 1970s.[4–6] TEM was used for many subsequent structural studies of core–shell latex particles.[1,7–13] Other methods, like small angle neutron[12,14,15] or X-ray[16–18] scattering, high-resolution NMR,[19,20] or titration methods,[21,22] were also used. Dynamic mechanical spectroscopy measurements[23–25] and atomic force microscopy[26] gave other evidence for the existence of structured core–shell particles. Recently, fluorescence nonradiative energy transfer (NRET) was used to investigate the internal structure of core–shell particles.[27,28]

In contrast to the internal structure, the rates and mechanism of film formation of core–shell particles have been only scarcely investigated so far. The only extensive studies were done using the NRET method.[29–31] They showed that the rates of polymer chain migration in dry films of acrylate core–shell latex particles can give useful information on the internal structure of the particle. For such particles, the TEM, for instance, could not be easily employed, since a selective staining of the core or of the shell of the particles was hard to achieve. The NRET method appeared, therefore, particularly useful for the study of the internal structure of core–shell particles whose core and shell are made of the same type of polymer.

The present study concerns core–shell latex particles whose core is formed of poly(butylmethacrylate) (PBMA) and the shell of poly(butyl methacrylate-*co*-butyl acrylate-*co*-trifluoroethyl methacrylate) (PBBT). The ultimate goal in synthesizing these structured particles is to use only very little fluorinated monomer and to obtain most of the fluorinated copolymer at the surface of the final film, which will then be more hydrophobic than an entirely hydrogenated film. In the present study, we investigated the internal structure of these core–shell particles using particles with different shell thickness and different labeling of the core and of the shell.

EXPERIMENTAL

Materials

The monomers, butyl acrylate (BA) and trifluoroethyl methacrylate (TFEM), were gifts from Atochem, styrene (St) was a gift from the EAHP (Strasbourg), and butyl methacrylate (BMA) was purchased from Aldrich. The initiators, potassium persulfate (KPS), was purchased from Aldrich. Sodium hydrogen carbonate ($NaHCO_3$) was from Prolabo and the surfactant, sodium dodecyl sulfate (SDS), from Touzard and Matignon. SDS was recrystallized thrice from mixtures of water and ethanol. All other compounds were of the best grade available. The donor, (9-phenanthryl)-methyl methacrylate (PheMMA), and the acceptor, 9-anthryl methacrylate (AnMA), were synthesized following the recipe given elsewhere.[32] Water was freshly deionized and distilled before use.

Latex Synthesis

The latex particles were synthesized by semicontinuous free-radical emulsion polymerization using potassium persulfate as the initiator and following a procedure described by Zhao et al.[32] For the synthesis of the homogeneous particles, a latex seed was first prepared and the rest of the components, including the donor (PheMMA) or the acceptor (AnMA), was next slowly (starving conditions) added to the seed. For the synthesis of the composite (core–shell) particles, a latex seed was first prepared and, next, the rest of the components was slowly added in two steps. The donor or the acceptor was added during the first slow step following the seed and, in some cases, during the second slow step. This second step was started 1 h after the end of the addition of the components of the previous step, to let all the monomer of the core to be consumed before starting to build up the shell. During this period of time, the emulsion was maintained at the temperature of the polymerization, 80°C. In each of the slow steps, the aqueous phase (containing the KPS and the SDS) and the organic phase (the monomers)

Table I Recipes and Polymerization Conditions for the Homogeneous (H1 and H2) and Core–Shell (CS1 and CS8) Latex Synthesis

Step	Composition (g)	H1	H2	CS1	CS2	CS3	CS4	CS5	CS6	CS7	CS8
Seed (batch)											
(80°C)	Water	45.1	45	45.2	44.8	45.1	44.9	45.2	45.1	44.9	45.1
	KPS	0.0429	0.0427	0.0428	0.0428	0.0429	0.0428	0.0426	0.0429	0.0428	0.0427
	SDS	0.0308	0.0303	0.0305	0.0306	0.0307	0.0305	0.0307	0.0305	0.0306	0.0307
	$NaHCO_3$	0.0816	0.082	0.0818	0.0815	0.0816	0.0818	0.082	0.0819	0.0816	0.0817
	BMA	2.93	2.92	2.93	2.93	2.92	2.93	2.93	2.92	2.93	2.93
First slow step											
(5 h) (80°C)	Water	14.03	13.94	14.02	14.1	13.98	14.01	10.01	9.97	10.12	10.05
	KPS	0.025	0.0255	0.0247	0.0252	0.0248	0.0251	0.0181	0.0178	0.0182	0.0183
	SDS	0.24	0.2	0.235	0.21	0.242	0.202	0.142	0.139	0.140	0.141
	BMA	15.72	15.75	15.68	15.65	15.75	15.71	11.56	11.54	11.55	11.57
	PheMMA	0.304		0.305		0.303		0.224		0.223	
	AnMA		0.289		0.292		0.288		0.213		0.212
Second slow step											
(5 h) (80°C)	Water			6.1	6.02	6.05	5.98	10.2	10.05	9.98	10.01
	KPS			0.0105	0.0112	0.0108	0.011	0.018	0.0178	0.0181	0.018
	SDS			0.101	0.0802	0.1	0.0805	0.141	0.1396	0.1405	0.1402
	BMA			1.28	1.282	1.278	1.281	2.19	2.185	2.191	2.188
	BA			1.412	1.408	1.407	1.411	2.411	2.408	2.412	2.407
	TFEM			4.042	4.06	4.038	4.051	6.92	6.93	6.93	6.92
	PheMMA			0.122				0.2086			
	AnMA				0.1154				0.192		

were added separately to the reactor. These slow steps were performed in about 5 h each; next, the dispersion was left at 80°C, with gentle stirring, for an additional 10 h. The molar concentration ratio [donor or acceptor]/[monomer] was 0.01.

The homogeneous particles are made of poly(butyl methacrylate) (PBMA). The core of the core–shell particles was made of pure PBMA, and the shell of the statistical copolymer, of poly(butyl methacrylate-*co*-butyl acrylate-*co*-trifluoroethyl methacrylate) (PBBT). The composition of the PBBT was 60, 21, and 19 wt % or 54.6, 25, and 20.4 mol % of TFEM, BA, and BMA, respectively. This composition of the shell was chosen in such a way that its T_g matches the T_g of the core, equal to 34 ± 3°C. The recipes and polymerization conditions are given in Table I, and the main characteristics of these latexes are reported in Table II.

Tables I and II indicate that two types of core–shell particles were synthesized which differ by the way the core and the shell of the particles have been labeled. They are schematically represented in Figure 1. In Type I, the core and the shell were labeled with the same probe, the donor in latex CS1 and CS5 and the acceptor in latex CS2 and CS6 (see Table II). In Type II, only the cores of the particles were labeled (CS3, CS4, CS7, and CS8). Finally, the two homogeneous PBMA latexes synthesized contain either the donor (H1) or the acceptor (H2) of energy. Proper labeling of the polymer chains was checked using a UV detector coupled to a GPC apparatus.

Latex Particle-size Measurements

Films were prepared by casting 2–3 drops of dispersion (25 wt% solid content) onto freshly cleaved mica plates and allowed to air dry. Particle diameters were determined from the height profile (see Fig. 2) on latex dry films by atomic force microscopy (AFM) working in the height mode, which means that the force exerted on the film by the cantilever during scanning was kept constant. The diameter of the particles was obtained from the average distance between the center of two adjacent particles (represented by the triangles in Fig. 2b), using the AFM software. For each latex studied, at least 30 values were measured to obtain the average diameters given in Table II. The accuracy in the determination of the particle diameter is around 5%. The AFM used was a Nanoscope III from Digital Instruments, Inc., Santa Barbara, CA. The piezoelectric translator could scan a maximum surface area of 12

Table II Symbols Used in the Text, Composition, and Diameter of the Particles Measured by AFM and Theoretical Core Radius and Shell Thickness for the Synthesized Latex Particles

Latex	Theoretical Structure (Wt %)	Chemical Composition		Measured Particle Diameter (nm)	Theoretical	
		Core	Shell		Core Radius[a] (nm)	Shell Thickness[b] (nm)
H1	Homogenous 100	PBMA(Phe)		232	—	—
H2	Homogenous 100	PBMA(An)		220	—	—
CS1 (Type I)	Core–shell 74-26	PBMA(Phe)	PBBT(Phe)	232	105	11
CS2 (Type I)	Core–shell 74-26	PBMA(An)	PBBT(An)	234	106	11
CS3 (Type II)	Core–shell 74-26	PBMA(Phe)	PBBT	269	122	13
CS4 (Type II)	Core–shell 74-26	PBMA(An)	PBBT	249	113	12
CS5 (Type I)	Core–shell 56-44	PBMA(Phe)	PBBT(Phe)	226	93	20
CS6 (Type I)	Core–shell 56-44	PBMA(An)	PBBT(An)	240	99	21
CS7 (Type II)	Core–shell 56-44	PBMA(Phe)	PBBT	230	95	20
CS8 (Type II)	Core–shell 56-44	PBMA(An)	PBBT	258	106	23

(Phe) stands for phenanthrene-labeled polymer chains, and (An), for anthracene-labeled polymer chains.
[a] Calculated from the measured particle diameter and the quantity of core–polymer introduced during the synthesis.
[b] Calculated from the measured particle diameter and the quantity of shell–polymer introduced during the synthesis.

$\times$ 12 μm^2. The spring constant of the cantilever was 0.58 N m^{-1}. Besides the determination of the particle diameter, AFM allows one to appreciate the shape and the polydispersity of the particles and to follow the evolution of the particle size during synthesis (an example is shown in Fig. 3). AFM images revealed that all particles investigated in this study were spherical with a very low polydispersity in size and that no second nucleation had appeared. Indeed, the increase in the size of the particles during the synthesis was found to be in agreement with the amount of monomer introduced during the first and the second slow steps of the polymerization assuming that the number of particles did stay constant. This control was necessary to give a reliable interpretation to the fluorescence data. Indeed, our interpretation rests on the assumption that the particles are spherical and that no second nucleation has occurred, in particular during the synthesis of the shell.

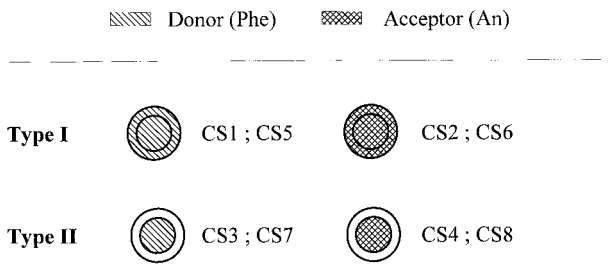

Figure 1 Schematic representation of the two types of core–shell latexes used in this work.

Latex Films for Energy-transfer Measurements

Films used for the study of polymer chain migration were prepared by mixing stoichiometrically the corresponding donor- and acceptor-labeled latex particles and by casting 2–3 drops of the mixed dispersion (25 wt% solid content) onto quartz plates and allowed to air dry. Dry films were about 100 μm thick. Films were kept under argon during annealing. Annealing was made at 90°C for various periods of time (see Figs. 6–9 for annealing times). After each period of annealing, the fluorescence decays were recorded by keeping the films at 10°C, which is much below the T_g of the polymers, to avoid any kind of chain migration during the fluorescence decay measurements.

Fluorescence Decay Measurements

Phenanthrene (donor) fluorescence decay traces were recorded with a single photon counting apparatus.[33] The film samples, mounted on a homemade solid holder, were excited at 298 nm. The emission light was collected through a band pass

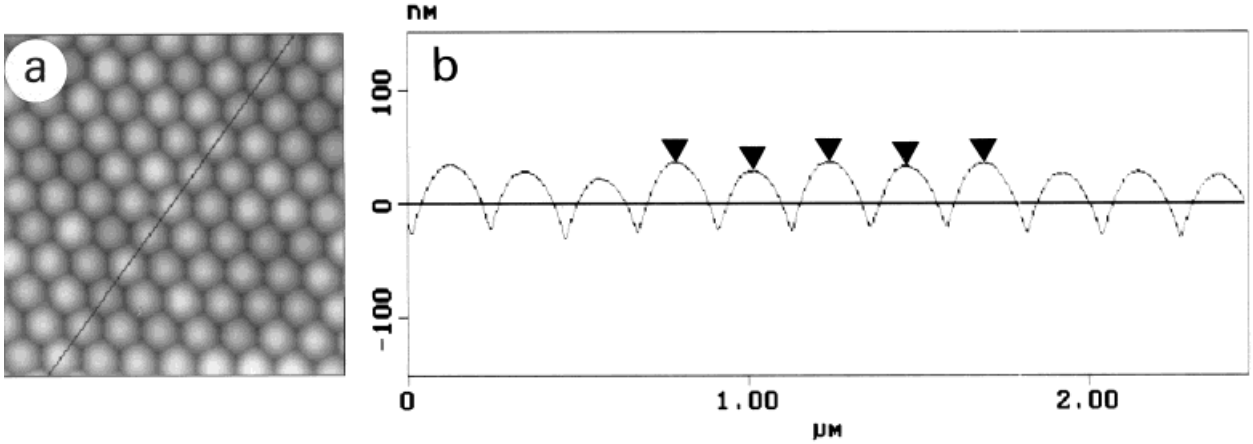

Figure 2 (a) AFM top view (size: 2 × 2 μm^2) of a CS2 latex film and (b) height profile taken along the line shown on the top view image.

filter (Schott) centered at 366 nm to minimize the uptake of scattered and acceptor (anthracene) emitted light.

ANALYSIS OF THE FLUORESCENCE DECAY CURVES AND MODELING OF FILM FORMATION

Analysis of the Fluorescence Decay Curves from Latex Film

Several analyses of the donor fluorescence decay data obtained using the nonradiative energy transfer method to follow polymer chain interdiffusion across an interface were proposed. Winnik and collaborators were the first to use fluorescence nonradiative energy transfer for the study of polymer chain diffusion in latex films.[29,32,34–38] In their model, they assumed that donor- and acceptor-labeled polymer chains are distributed into three domains as shown in Figure 4. In domains 1 and 2, no mixing has yet occurred during annealing. These domains contain the donor (domain 1) and the acceptor (domain 2) alone. In domain 3, donor- and acceptor-labeled polymer chains are mixed, as a result of interparticle chain diffusion, and energy transfer occurs in this domain. Thus, the donor fluorescence intensity decay is due to the two distinct domains 1 and 3. Although this approach is an approximation, it was shown to be very useful in the study of latex film formation.[27–32,34–42]

More recently, other models were proposed to improve the analysis of the fluorescence decay data. These models mainly take into account the fact that, in contrast to the model shown in Figure 4, there is not a sharp front between unmixed and mixed domains. Indeed, a nonuniform concentration profile of the donor- and acceptor-labeled

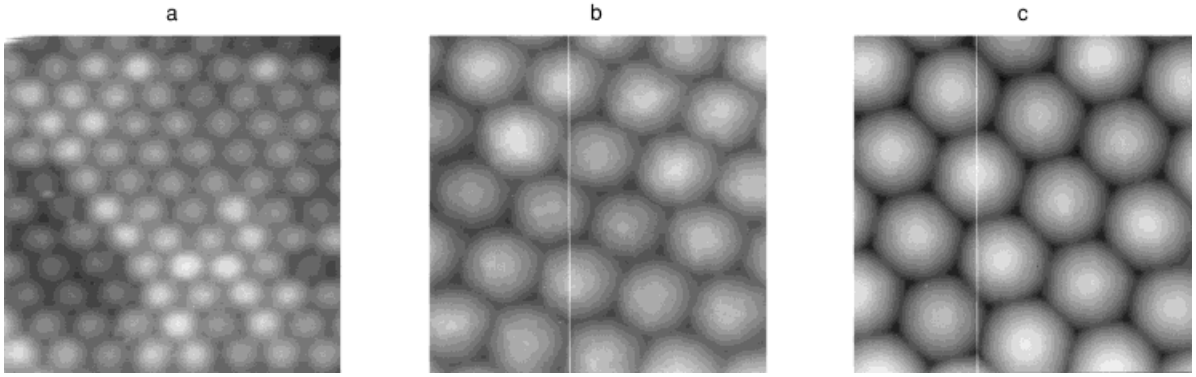

Figure 3 AFM top views of CS4 latex films during synthesis: (a) after formation of the seed; (b) after formation of the core; (c) the core–shell particles at the end of the synthesis. Images size: 1 × 1 μm^2.

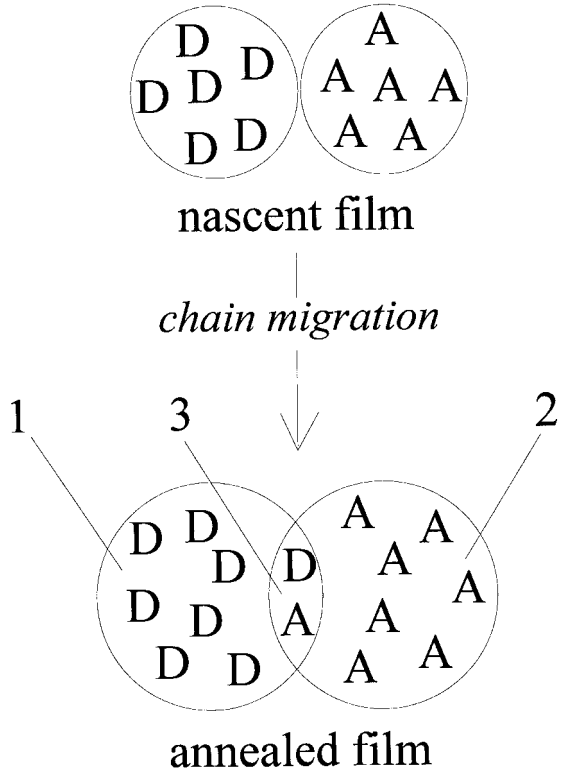

Figure 4 Schematic representation of the earlier model proposed by Winnik and collaborators[32,34,35] for the interpretation of the polymer chain diffusion in latex films.

polymer chains develops during film annealing. Models were proposed along this line which lead, for instance, to the recovery of the acceptor or of the donor concentration profile during film annealing.[43,44] Use of these models implies a very low concentration of donor-labeled particles compared to the concentration of the acceptor-labeled particles in the film. Under this condition, we had very weak signals, leading to imprecise fitting parameters. Yekta et al.[45] gave a general equation of the fluorescence decay under the condition where the donor and acceptor have a nonuniform concentration profile but which is of planar symmetry. Interesting simulations of the donor fluorescence intensity decay were done by Dhinojwala and Torkelson.[46] Assuming a Fickian diffusion of the polymer chains through a planar interface, they showed that the fluorescence intensity decay provides excellent sensitivity for determining the polymer self-diffusion coefficient. They also proposed to use the normalized efficiency of energy transfer, coupled with a Fickian concentration profile of the donors and acceptors, to analyze the fluorescence transient data. The final result of their calculation shows that the simplified formalism used by Winnik and collaborators underestimates the effective polymer self-diffusion coefficient. It will be seen that the absolute value of the polymer diffusion coefficients is not involved in our study.

The analysis of the decay data, collected in the present work for various nascent or annealed films, was done as proposed in their first reports by Winnik and collaborators.[32,34,35] It has the advantage of simplicity, and although it is less sophisticated than more recent models, it gives good information on the internal structure of the synthesized core–shell particles, as will be seen in the following. This analysis is derived from the Förster equation[47] of nonradiative energy transfer and based on the fact that the donors and the acceptors are static during the fluorescence measurements. The efficiency of the energy transfer is governed by the relation $E = R_0^6/(R_0^6 + r^6)$, where R_0 is the characteristic distance between donor and acceptor, equals 23 Å for the couple phenanthrene–anthracene used in the present study, and r, the distance between the donor and the acceptor. Thus, the energy transfer depends only on the average donor–acceptor distance in the range 0–50 Å, which is small compared to the particle sizes (see Table II).

The donor fluorescence decay $I(t)$ is expressed by the sum of two contributions, weighted by the preexponential factors B_1 and B_2, one which comes from the domains where the donor is mixed with the acceptor and the other which comes from the domains where the donor is without any acceptor in its vicinity (see Fig. 4), respectively:

$$I(t) = B_1 \exp[(-t/\tau) - p(t/\tau)^{1/2}] + B_2 \exp(-t/\tau) \quad (1)$$

In eq. (1), p is a time-independent parameter proportional to the local concentration of acceptor, and τ, the donor fluorescence lifetime that was found equal to 46 ns in film containing only donor-labeled particles. The parameters B_1, B_2, and p are obtained by fitting eq. (1) to the fluorescence decay data using a nonlinear weighted least-squares procedure. An apparent volume fraction of mixing f'_m was defined from B_1 and B_2,[32,34,35] which is equal to

$$f'_m = B_1/(B_1 + B_2) \quad (2)$$

This fraction was corrected for energy transfer

taking place through a perfectly sharp interface between the donor- and the acceptor-labeled domains [$f'_m(i)$] and for energy transfer which occurs when the donor and acceptor domains are fully mixed [$f'_m(\infty)$] and replaced by a normalized volume fraction of mixing f_m given by eq. (3):

$$f_m = [f'_m - f'_m(i)]/[f'_m(\infty) - f'_m(i)] \qquad (3)$$

The volume fraction of mixing $f'_m(i)$ was measured using nascent films formed from a stoichiometric mixture of donor- and acceptor-labeled particles and found to be very close to the theoretical value calculated from the known particle size (between 0.14 and 0.2 for the particles of Type I and between 0.05 and 0.1 for the particles of Type II). The volume fraction of mixing $f'_m(\infty)$ corresponds to fully mixed donor- and acceptor-labeled polymer chains. It was obtained from a latex film formed from a stoichiometric mixture of donor- and acceptor-labeled particles, dissolved in THF, and solution-cast onto a quartz plate and found to be close to 0.97. This volume fraction of mixing is also the volume fraction of mixing which can be found at an infinite annealing time of the film.

Modeling of Film Formation

We have assumed, as done in other studies of film formation,[29–32,34–38] that chain migration upon film annealing follows a Fickian diffusion. The concentration profile of the donor, at annealing time t, is then given by relation (4) (Ref. 32):

$$C_D(r, t) = \frac{C_0}{2}\left[\operatorname{erf}\left[\frac{R + r}{2(Dt)^{0.5}}\right] + \operatorname{erf}\left[\frac{R - r}{2(Dt)^{0.5}}\right]\right] - \frac{C_0}{r}\left(\frac{Dt}{\pi}\right)^{0.5}\left[\exp\left[-\frac{(R - r)^2}{4Dt}\right] - \exp\left[-\frac{(R + r)^2}{4Dt}\right]\right] \qquad (4)$$

where R is the particle radius, and D, the polymer chain diffusion coefficient. This relation is valid for the particles of Types I and II as well, but with R_c (radius of the core) instead of R for the particles of Type II. C_0 is the initial, homogeneous, donor concentration at time $t = 0$ in the particles of Type I (C_0^{I}) and in the core of the particles of Type II (C_0^{II}). The fractions of mixing, represented in Figure 5 for the particles of Types I and II, are therefore given by

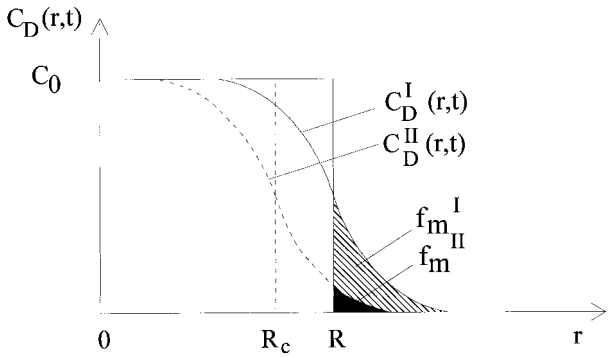

Figure 5 Schematic representation of the donor concentration profile $C_D(r, t)$ vs. the distance, r, from the center of the particle, for the core–shell particles of Types I and II during film formation.

$$f_m^{\mathrm{I}} = \frac{3}{4\pi R^3}\int_R^\infty \frac{C_D^{\mathrm{I}}(r, t)}{C_0^{\mathrm{I}}}\,4\pi r^2\,dr \qquad (5)$$

and

$$f_m^{\mathrm{II}} = \frac{3}{4\pi R_C^3}\int_R^\infty \frac{C_D^{\mathrm{II}}(r, t)}{C_0^{\mathrm{II}}}\,4\pi r^2\,dr \qquad (6)$$

respectively. In these equations, $C_D^{\mathrm{I}}(r, t)$ and $C_D^{\mathrm{II}}(r, t)$ represent the concentration profiles of the donor (see Fig. 5) in the films of Types I and II at time t, respectively, given by eq. (4).

RESULTS AND DISCUSSION

Typical donor (phenanthrene) fluorescence decay curves in latex films were already presented in several articles.[32,35–38] Similar decay curves were obtained in the present work and will not be shown. In Figures 6 and 7, we give the variations of the volume fraction of mixing f_m, deduced from the decay curves using eq. (3), in films of homogeneous and core–shell particles annealed at 90°C. Recall that each film was formed from a stoichiometric mixture of phenanthrene- and anthracene-labeled particles, which were either completely labeled (Type I) or only labeled in the core (Type II). Indeed, the labeling of the core and of the shell of the particle does not give any contrast between the diffusion of the core and the shell of the particles since the core and the shell have the same T_g. On the contrary, as will be shown,

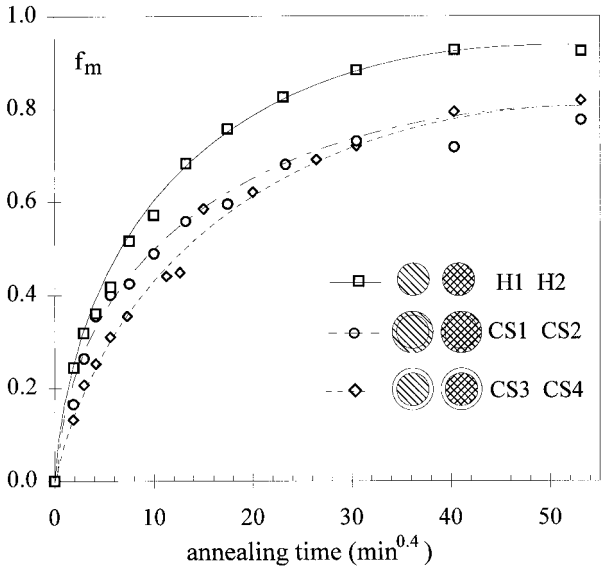

Figure 6 Volume fraction of mixing vs. annealing time at 90°C for films of particles (□) H1–H2, (○) CS1–CS2, and (◇) CS3–CS4. The lines are guides for the eyes.

comparison between the results obtained with the particles of Types I and II gives evidence that a great part of the polymer which should theoretically form the shell of the particles is indeed located at the periphery of the particles.

Figure 6 shows the variation of f_m vs. annealing time for the mixtures of particles H1 and H2, CS1 and CS2, and CS3 and CS4. The general trend of the three variations are similar. One observes an increase of the volume fraction of mixing with increase of the annealing time, as is generally the case. However, one observes also a decrease of f_m at a constant annealing time going from the homogeneous latex particles to the core–shell particles. This decrease can be attributed to the presence of a shell around the particles which gives rise to a delay in the measured fraction of mixing and, therefore, to a shift of the f_m vs. annealing time curves, as explained now.

H1–H2 and CS1–CS2 films are made of completely labeled particles. Therefore, the delay which is observed going from the H1–H2 film to the CS1–CS2 film comes probably from a partial incompatibility between the polymers forming the core and the shell of the CS1 and CS2 particles, which slows down chain migration. One can think that this incompatibility should appear, on the f_m vs. annealing time curve, only after chain migration has covered a shell thickness. Below this migration distance, the curve of the core–shell particle should closely follow the curve corresponding to the homogeneous particle and should deviate only above this migration distance, when incompatibility becomes effective. In fact, as shown for other core–shell latex particles,[27,28] and in a recent study of the internal structure of core–shell particles similar to those synthesized here,[48] there is certainly not a sharp interface between the core and the shell of the particles. There is, rather, a concentration gradient of the shell– and core–polymer, from the surface to the center of the particle. Therefore, some incompatibility must already exist during the first steps of chain migration. This can explain the lower values of f_m for the CS1–CS2 film, compared to the f_m values found for the H1–H2 film, at a short annealing time.

On the other hand, the decrease of f_m observed when going from the CS1–CS2 film to the CS3–CS4 film, at annealing times below 80 h, is easy to explain. Indeed, there is no labeling of the shell in the CS3 and CS4 particles. Therefore, the diffusion process which involves the shell of the CS3 and CS4 particles cannot be detected in the fluorescence measurements, even though polymer chain migration occurs in the shell during annealing. Thus, the curve f_m vs. annealing time for the CS3–CS4 film presents an apparent delay when compared to the curve obtained for the CS1–CS2 film.

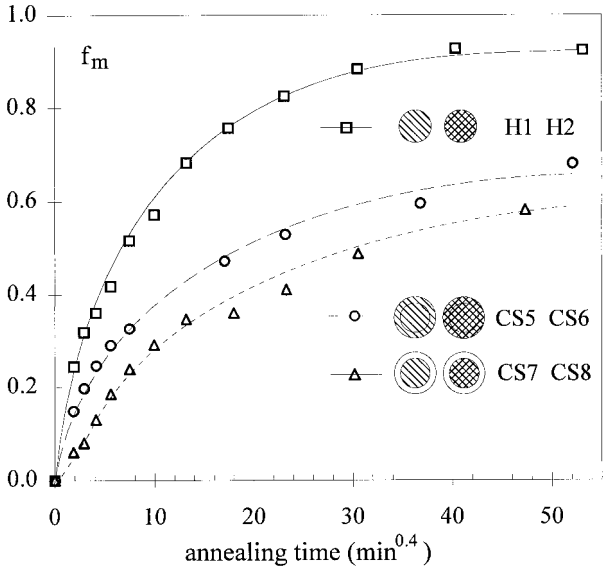

Figure 7 Volume fraction of mixing vs. annealing time at 90°C for films of particles (□) H1–H2, (○) CS5–CS6, and (△) CS7–CS8. The lines are guides for the eye.

The observations made with the CS1–CS2 and CS3–CS4 films are confirmed with the results shown in Figure 7. Notice that the shell thickness of latexes CS5 to CS8 is about twice the shell thickness of latexes CS1 to CS4, and latexes CS7 and CS8 are only labeled in the core (see Table II). The decrease observed in Figure 7 from one core–shell film to another is larger than in Figure 6. This comes from the larger shell thickness synthesized in the CS5 to CS8 latexes compared to the shell thickness in the CS1 to CS4 latexes. The results in Figures 6 and 7 seem, therefore, to indicate that the shell–polymer is indeed located at the periphery of the particles. If core–shell particles would not have been synthesized, the curves for the core–shell particles in Figures 6 and 7 would have been superimposed.

Another comment can be made which concerns the value of f_m at a long annealing time in Figures 6 and 7. One observes that f_m reaches different plateau values, the largest one, close to 1, is for the H1–H2 film and the lowest one, close to 0.6, is for the CS7–CS8 film. The variation of the plateau values shown in Figures 6 and 7 can also been explained by the presence, in the core–shell particles, of a shell made of a polymer of a different nature than the polymer in the core. Due to some incompatibility between the two types of polymers (PBMA presumably at the center and the copolymer PBBT at the periphery), it turns out that after some annealing time chain migration becomes hindered and, therefore, f_m reaches a plateau value lower than 1. Moreover, the core–shell particles in Figure 7 have a lower plateau value than that of the core–shell particles in Figure 6. This is in agreement with the larger shell thickness of the core–shell particles in Figure 7. Indeed, these particles offer a more efficient barrier to the interpenetration of the chain belonging to the core of adjacent particles than do the core–shell particles in Figure 6, which possess a thinner shell thickness. Only in the case of the homogeneous particles H1 and H2 is the interdiffusion between the chain belonging to adjacent particles complete (plateau value close to 1 in Figs. 6 and 7) since then the polymer chains belonging to adjacent particles are the same and there is, therefore, no hindrance for the migration of the chains which could arise from a thermodynamic incompatibility. In summary, all the results shown in Figures 6 and 7 concur to indicate that the particles CS1 to CS8 have probably a structure close to the desired core–shell structure.

To strengthen this conclusion, the values of f_m for the particles with the unlabeled shell (Type II) have been simulated from the experimental values of f_m found with the completely labeled core–shell particles (Type I), using the model given in Figure 5. Recall that in this model R_c is the radius of the core of a particle of radius R and $C_D^{\mathrm{I}}(r,t)$ and $C_D^{\mathrm{II}}(r,t)$ represent the concentration profile of the donor for the Types I and II core–shell particles, respectively, as a function of the distance, r, from the center of the particle, at a annealing time t. The theoretical thickness, e, of the shell of the particles is given by $R - R_c$. C_0 is the initial donor concentration, after synthesis and before film annealing, in the core (Type II) or in the whole particle (Type I). The same donor concentration was used in the synthesis of all particles. The black and the striped parts in Figure 5 represent the polymer chains which have left the original latex particle, and, therefore, f_m^{I} and f_m^{II} are the fraction of mixing for the particles of Types I and II, respectively.

From the experimental values of $f_m(f_m^{\mathrm{I}})$ at time t for the CS1–CS2 and CS5–CS6 films (see Figs. 6 or 8 and 7 or 9 for film CS1–CS2 and film CS5–CS6, respectively), we calculated the values of D which satisfy eqs. (4) and (5). These values

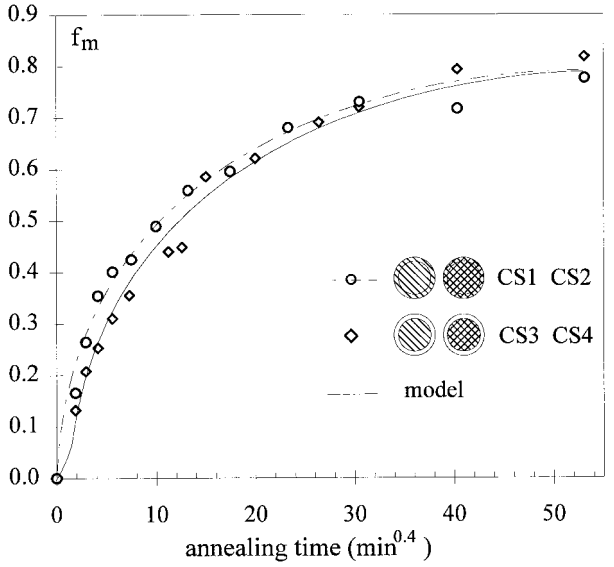

Figure 8 Volume fraction of mixing vs. annealing time at 90°C for films of particles (○) CS1–CS2, and (◇) CS3–CS4. The dashed line is a guide for the eyes for the CS1–CS2 film, and the continuous line is the variation of the volume fraction of mixing for the CS3–CS4 film predicted from the model as described in the text.

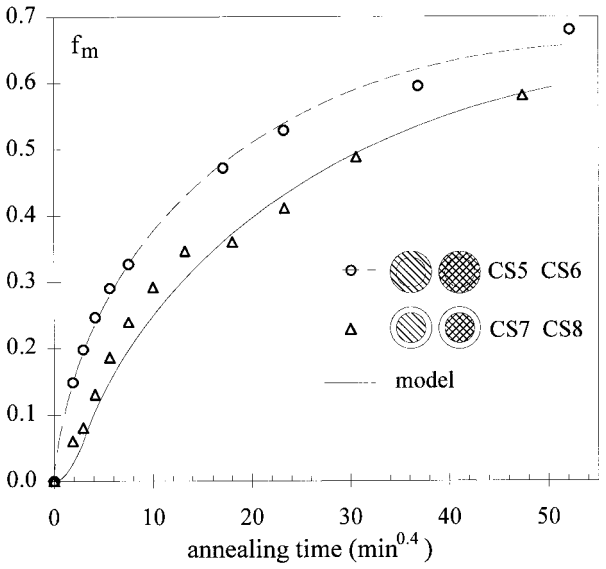

Figure 9 Volume fraction of mixing vs. annealing time at 90°C for films of particles (○) CS5–CS6, and (△) CS7–CS8. The dashed line is a guide for the eyes for the CS5–CS6 film, and the continuous line is the variation of the volume fraction of mixing for the CS7–CS8 film predicted from the model as described in the text.

were next introduced into eqs. (4) (with $R = R_c$) and (6), which then provided the theoretical values of $f_m(f_m^{II})$ at time t for the core–shell particles of Type II (CS3–CS4 and CS7–CS8), assuming the same diffusion coefficient, D, for the polymer chains belonging to the particles of Types I and II. The results are given in Figures 8 and 9 where the continuous curves represent the theoretical variations of f_m, f_m^{II}, vs. annealing time for the polymer chains in the CS3–CS4 (Fig. 8) and in the CS7–CS8 (Fig. 9) films (for the sake of clarity, the discrete theoretical values of f_m has been replaced by a smooth continuous curve). The agreement between the predicted variations of f_m and the experimental data is quite remarkable. This result strongly tends to indicate that the synthesis has led to the formation of core–shell latex particles. However, as pointed out already above, there is probably not a sharp interface between the polymer which is expected to form the core and the shell of the particles. Therefore, we undertook fluorescence measurements using particles which were carrying a different probe in the core (the donor or the acceptor) and in the shell (the acceptor or the donor), in order to quantify the thickness of the interface between the core and the shell of the particles. The results concerning this work will be reported elsewhere.[48]

CONCLUSION

The aim of this work was to obtain information on the internal structure of core–shell latex particles. For this purpose, we used the NRET method which has been previously extensively employed for the study of chain migration between adjacent latex particles during film formation. We studied film formation with core–shell particles which were labeled with an energy donor and an energy acceptor either in the whole particle or only in the core. An AFM image of all the particles synthesized was also taken to check that no second nucleation had occurred during the synthesis and, particularly, during the second step, when the shell was synthesized. It was also very important to ascertain that the final particle was spherical. If a second nucleation would have taken place, or if no spherical particles would have been formed, our interpretation of the fluorescence data would have been meaningless.

We have shown that the monomers introduced during the synthesis of the shell form a polymer situated mainly on the outside layer of the particles. This conclusion was obtained from (i) the comparison between the rate of film formation for homogeneous particles and core–shell particles and (ii) the analysis of the rate of film formation using a spherical Fickian model of diffusion for the polymer chains of the core–shell particles carrying different types of labeling. This work shows, on a more general basis, a way to use the NRET method to gain information on the internal structure of core–shell latex particles. This method is particularly useful when the core and the shell of the particles are composed of polymers of a similar nature.

P. M. thanks Elf Atochem for its financial support and its interest in this work.

REFERENCES

1. G. A. Vandezande and A. Rudin, *J. Coat. Technol.,* **66,** 99 (1994).
2. D. C. Sundberg, A. P. Casassa, J. Pantazopoulos, M. R. Muscato, B. Kronberg, and J. Berg, *J. Appl. Polym. Sci.,* **41,** 1425 (1990).

3. E. J. Sundberg and D. C. Sundberg, *J. Appl. Polym. Sci.,* **47,** 1277 (1993).
4. M. R. Grancio and D. J. Williams, *J. Polym. Sci., A,* **1,** 2617 (1970).
5. P. Keusch and D. J. Williams, *J. Polym. Sci. Polym. Chem. Ed.,* **11,** 143 (1973).
6. G. Kanig and H. Neff, *Colloid Polym. Sci.,* **253,** 29 (1975).
7. M. Okubo, Y. Katsuta, and T. Matsumoto, *J. Polym. Sci. Polym. Lett. Ed.,* **20,** 45 (1982).
8. T. I. Min, A. Klein, M. S. El-Aasser, and J. W. Vanderhoff, *J. Polym. Sci. Polym. Chem. Ed.,* **21,** 2845 (1983).
9. Y.-C. Chen, V. Dimonie, and M. S. El-Aasser, *Macromolecules,* **24,** 3779 (1991). Y.-C. Chen, V. L. Dimonie, O. L. Shaffer, and M. S. El-Aasser, *Polym. Int.,* **30,** 185 (1993).
10. J.-E. Jönsson, H. Hassander, and B. Törnell, *Macromolecules,* **27,** 1932 (1994).
11. W. He, J. Tong, M. Wang, C. Pan, and Q. Zhu, *J. Appl. Polym. Sci.,* **55,** 667 (1995).
12. W.-H. Hergeth, H.-J. Bittrich, F. Eichhorn, S. Schlenker, K. Schmutzler, and U.-J. Steinau, *Polymer,* **60,** 1913 (1989).
13. S. Kamei, M. Okubo, and T. Masumoto, *J. Polym. Sci. Polym. Chem. Ed.,* **24,** 3109 (1986).
14. J. M. O'Reilly, S. M. Melpolder, L. W. Fischer, G. D. Wignall, and V. Ramakrishnan, *Polym. Prepr. Am. Chem. Soc. Div. Polym. Chem.,* **24,** 407 (1983). L. W. Fischer, S. M. Melpolder, J. M. O'Reilly, V. Ramakrishnan, and G. D. Wignall, *J. Colloid Interf. Sci.,* **123,** 24 (1988).
15. M. P. Wai, R. A. Gelman, M. G. Fatica, R. H. Hoerl, and G. D. Wignall, *Polymer,* **28,** 918 (1987).
16. R. Grunder, G. Urban, and M. Ballauff, *Colloid Polym. Sci.,* **271,** 563 (1993).
17. N. Dingenouts and M. Ballauff, *Acta Polym.,* **44,** 178 (1993).
18. M. Ballauff, *Macromol. Symp.,* **87,** 93 (1994).
19. D. Tembou Nzudie, L. Delmotte, and G. Riess, *Makromol. Chem. Rapid Commun.,* **12,** 251 (1991).
20. D. Tembou Nzudie, L. Delmotte, and G. Riess, *Macromol. Chem. Phys.,* **195,** 2723 (1994).
21. F. Dobler, T. Pith, Y. Holl, and M. Lambla, *J. Appl. Polym. Sci.,* **44,** 1075 (1992).
22. S. Muroi, H. Hashimoto, and K. Hosoi, *J. Polym. Sci. Polym. Chem. Ed.,* **22,** 1365 (1984).
23. S. C. Misra, C. Pichot, M. S. El-Aasser, and J. W. Vanderhoff, *J. Polym. Sci. Polym. Lett. Ed.,* **17,** 567 (1979).
24. S. C. Misra, C. Pichot, M. S. El-Aasser, and J. W. Vanderhoff, *J. Polym. Sci. Polym. Chem. Ed.,* **21,** 2383 (1983).
25. J. Y. Cavaillé, C. Jourdan, X. Y. Kong, J. Perez, C. Pichot, and J. Guillot, *Polymer,* **27,** 693 (1988).
26. F. Sommer, Tran Min Duc, R. Pirri, G. Meunier, and C. Quet, *Langmuir,* **11,** 440 (1995).
27. M. A. Winnik, H. Xu, and R. Satguru, *Makromol. Chem. Macromol. Symp.,* **70/71,** 107 (1993).
28. E. Pérez and J. Lang, *Langmuir,* **12,** 3180 (1996).
29. H.-B. Kim, Y. Wang, and M. A. Winnik, *Polymer,* **35,** 1779 (1994).
30. D. Juhué and J. Lang, *Macromolecules,* **28,** 1306 (1995).
31. D. Juhué and J. Lang, *Double Liaison-Phys. Chim. Peint. Adhes.,* **464–465,** 3 (1994).
32. C.-L. Zhao, Y. Wang, Z. Hruska, and M. A. Winnik, *Macromolecules,* **23,** 4082 (1990).
33. G. Pfeffer, H. Lami, G. Laustriat, and A. Coche, *C. R. Hebd. Séances Acad. Sci.,* **257,** 434 (1963).
34. Ö. Pekcan, M. A. Winnik, and M. D. Croucher, *Macromolecules,* **23,** 2673 (1990).
35. Y. Wang, C.-L. Zhao, and M. A. Winnik, *J. Chem. Phys.,* **95,** 2143 (1991).
36. Y. Wang, M. A. Winnik, and F. Haley, *J. Coat. Technol.,* **64,** 51 (1992).
37. Y. Wang and M. A. Winnik, *Macromolecules,* **26,** 3147 (1993).
38. Y. Wang and M. A. Winnik, *J. Phys. Chem.,* **97,** 2507 (1993).
39. Y. Wang and M. A. Winnik, *Macromolecules,* **23,** 4731 (1990).
40. D. Juhué, Y. Wang, and M. A. Winnik, *Makromol. Chem. Rapid Commun.* **14,** 345 (1993).
41. E. M. Boczar, B. C. Dionne, Z. Fu, A. B. Kirk, P. M. Lesko, and A. D. Koller, *Macromolecules,* **26,** 5772 (1993).
42. D. Juhué and J. Lang, *Macromolecules,* **27,** 695 (1994).
43. Y. S. Liu, L. Li, S. Ni, and M. A. Winnik, *Chem. Phys.,* **177,** 579 (1993).
44. Y. S. Liu, J. Feng, and M. A. Winnik, *J. Chem. Phys.,* **101,** 9096 (1994).
45. A. Yekta, J. Duhamel, and M. A. Winnik, *Chem. Phys. Lett.,* **235,** 119 (1995).
46. A. Dhinojwala and J. M. Torkelson, *Macromolecules,* **27,** 4817 (1994).
47. Th. Förster, *Ann. Phys. (Leipzig),* **25,** 55 (1948); *Discuss. Faraday Soc.,* **27,** 7 (1959).
48. P. Marion, G. Beinert, D. Juhué, and J. Lang, *Macromolecules,* **30,** 123 (1997).